

Journal Pre-proofs

Research papers

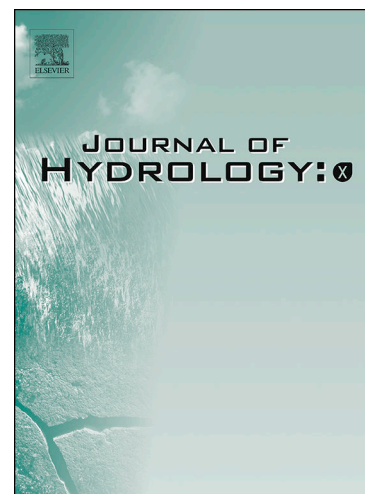
Water–soil interactions: unravelling the processes and stages involved in the wetting of water repellent soils

Helen M. Balshaw, Peter Douglas, Stefan H. Doerr

PII: S2589-9155(23)00011-1

DOI: <https://doi.org/10.1016/j.hydroa.2023.100158>

Reference: HYDROA 100158



To appear in: *Journal of Hydrology X*

Received Date: 30 May 2023

Revised Date: 28 July 2023

Accepted Date: 9 August 2023

Please cite this article as: H.M. Balshaw, P. Douglas, S.H. Doerr, Water–soil interactions: unravelling the processes and stages involved in the wetting of water repellent soils, *Journal of Hydrology X* (2023), doi: <https://doi.org/10.1016/j.hydroa.2023.100158>

This is a PDF file of an article that has undergone enhancements after acceptance, such as the addition of a cover page and metadata, and formatting for readability, but it is not yet the definitive version of record. This version will undergo additional copyediting, typesetting and review before it is published in its final form, but we are providing this version to give early visibility of the article. Please note that, during the production process, errors may be discovered which could affect the content, and all legal disclaimers that apply to the journal pertain.

© 2023 Published by Elsevier B.V.

1 **Water–soil interactions: unravelling the processes and stages involved in the wetting of**
2 **water repellent soils**

3

4 Helen M. Balshaw^{*1,2}, Peter Douglas^{3,4}, Stefan H. Doerr⁵

5 ¹College of Engineering, Swansea University, Bay Campus, Fabian Way, Crymlyn Burrows,
6 Swansea, SA1 8EN, UK

7 ²Present address: 1 Rosewarne Close, Llantilio Pertholey, Abergavenny, NP7 6QA.

8 ³Chemistry Group, College of Medicine; Swansea University, Singleton Park, Swansea SA2
9 8PP, UK; School of Chemistry and Physics, University of KwaZulu-Natal, Durban, RSA

10 ⁴Present address: The Conceptual Shed, 23 Meadow View, Dunvant, Swansea, SA2 7UZ, UK

11 ⁵Department of Geography, Swansea University, Singleton Park, Swansea, SA2 8PP, UK

12

13 ***Corresponding author:** email: hbalshaw@hotmail.co.uk

14

15 **Abstract**

16 Water repellent behaviour of soils is a widely studied phenomenon given its implications for
17 infiltration, runoff, erosion and preferential flow. However, the principles underlying the
18 eventual penetration of water into affected soils remain poorly understood. Theoretical
19 considerations of the energetics and kinetics involved as a water drop makes contact with a
20 water repellent soil surface and eventually penetrates into the soil suggest three distinct stages
21 in the overall process. These stages are 1) adhesional wetting as soil and water first make
22 contact, followed by 2) a kinetic barrier transitional stage in which molecular reorganisation of
23 organics on soil reduces the water-soil contact angle to allow the water drop to sit deeper over
24 soil particles of initial contact such that there is contact with particles in directly underlying
25 soil layers, and finally 3) branching interstitial wetting as water penetrates into the bulk soil.
26 Studies presented here of optical microscopy, mass of soil initially wetted, penetration time
27 through layers of soil of different thicknesses, and time-dependent measurements of contact
28 angle, volume of water penetrated, and mass of soil wetted, all give results consistent with this
29 model. However, only for highly water repellent soils can distinct stages in wetting be clearly
30 resolved experimentally, presumably because only these soils have a high enough kinetic
31 barrier in the transitional stage for good separation between stages. For less water repellent
32 soils, while the general time dependent behaviour remains consistent with the model, the
33 distinction between the three stages is not so easy to resolve experimentally. The roles of
34 contact angle, particle size distribution and drop size in determining the rates of these stages is
35 considered, and the implications of the model for understanding soil water repellency are
36 discussed.

37

38 **Keywords**

39 Soil physics, soil hydrophobicity, kinetics, contact angle, infiltration

40

41 **1. Introduction**

42 Soil water repellency is the reduced ability of affected soils to absorb water and become wetted.
43 It is thought to be caused by organic compounds with hydrophobic (non-polar) properties
44 present as coatings on soil grains (Roberts and Carbon, 1972; Bisdorn et al., 1993; Doerr et al.,
45 2000) and in interstitial matter (Franco et al., 2000). These compounds can be derived from
46 leaf surface waxes (McIntosh and Horne 1994), fungal and microbial activity (Jex et al., 1985;
47 Hallett et al., 2001), plant roots (Dekker and Ritsema 1996; Doerr et al., 1998) and lipids from
48 decomposing litter (McGhie and Posner, 1981) and lead to enhanced water repellency. It can
49 have substantial environmental consequences such as increased overland flow leading to soil
50 erosion, mass movement and flooding, especially after wildfires, as well as poor uptake of
51 agricultural chemicals (Doerr et al., 2000). The latter increases the risk of crop disease, reduces
52 yields and thus threatens food security and production (Bond, 1972). Soil water repellency also
53 increases the risk of groundwater pollution by accelerating transfer of contaminants and
54 nutrient leaching (Bisdorn et al., 1993; Ritsema and Dekker, 1996; Hallett et al., 2001) via
55 uneven wetting and preferential flow pathways (Dekker and Ritsema, 1994; Dekker et al.,
56 2000).

57 Two experimental methods for the assessment of soil water repellency commonly used are: the
58 water-soil contact angle, which is used to provide a measure of the initial water repellency; and
59 the Water Drop Penetration Time Test (WDPT) which measures the time for a water drop to
60 fully penetrate the soil (Letey, 1969; Doerr, 1998; Letey et al., 2000). When measuring soil
61 WDPT for previous studies (Balshaw et al., 2021) we often observed, particularly with highly
62 water repellent soils, that the process of water penetration appears to be a multistage process,
63 whereby initial contact of the water drop with the soil quickly initiates the lifting of soil grains
64 up and around the water drop, but this is then followed by an induction period where little
65 happens and the water drop sits on the soil until at some critical time there is more rapid
66 infiltration of the soil as if some kinetic barrier to infiltration has been overcome. We have been
67 intrigued by this behaviour over the years and curious to see if this multistage behaviour could
68 be quantified and understood from both theoretical and experimental viewpoints in order to
69 provide a conceptual model of what is involved when a water drop penetrates soil.

70 In general, we can envisage at least three stages in soil wetting. The initial process is the rapid
71 initial water/soil contact, i.e. adhesional wetting; the final process is branching interstitial
72 wetting as water penetrates the interstices of bulk soil; and whether or not an additional
73 intermediate stage, to transition between adhesional wetting and branching interstitial wetting,
74 is required depends on the initial degree of soil water repellency, i.e. the water-soil contact
75 angle. Shirtcliffe et al. (2006) have calculated a critical contact angle of 50° below which
76 adhesional wetting may lead immediately to interstitial wetting. While such low contact angles
77 may occur in soils of very low repellency, for soils of moderate to high water repellency, i.e.
78 those which have contact angles higher than this critical contact angle, there must also be an
79 intermediate process which allows the transition between these two wetting regimes. The
80 degree to which these three stages can be distinguished experimentally will depend, to a large
81 extent, on the soil water repellency.

82 In an attempt to understand these processes, and to determine if the stages could be
83 distinguished experimentally, we studied a number of sandy soils of differing water repellency
84 using a number of relatively simple techniques, described in detail in the following section,

85 which allow the complete process of wetting, from initial adhesional wetting through to the
86 end of branching interstitial wetting, to be followed. Goniometer time-lapse imaging, and
87 optical microscopy, were used to follow wetting by single drops in real time. A ‘start-stop’
88 method of collecting the mass of soil wetted at a given time after the drop was applied to the
89 soil was used by combining data from different drops at different stop times to give pseudo
90 time-lapse data with each data point obtained using a different water drop. A similar approach
91 was used in a study of the size and dimensions of the wetted water pellet as a function of time,
92 with the solid pellet obtained by freezing with liquid nitrogen. Experiments were also carried
93 out on water drop penetration times through soil layers of increasing thicknesses to build up
94 data on the rate of movement of the drop through the soil at various spatial stages in wetting.
95

96 **2. Materials and Methods**

97

98 *2.1 Materials*

99 Studies were primarily focused on four naturally water-repellent sandy soils of the type we
100 have used in previous work. Of these, three were from Gower, South Wales: two dune soils
101 from Nicholaston, NIC1 and NIC2, and a dune soil under pine forest from Llanmadoc, LLAN1,
102 and the other from the Netherlands, NL1, (Balshaw, 2019; Doerr et al., 2005). In addition to
103 these soils, a study of the size of wetted soil pellets as a function of time was made using a
104 sandy soil from Australia, AUC (wetable), which we have used in previous studies (Doerr et
105 al., 2005). It was chosen because it had a suitable WDPT for that particular experiment, and
106 the profilometry data shown in Figure 5 was obtained using a dune soil from Nicholaston,
107 Gower, UKC (wetable), and had previously been used by our group (Doerr et al. 2005). Soil
108 samples were taken from 0–10 cm depth. After collection, soils were oven dried at 30°C for 48
109 hr and then sieved using a 2-mm sieve to remove any large pieces of organic debris. Details of
110 the soils used are given in Table 1. Distilled water was used throughout.

111

112 *2.2 Methods*

113 *2.2.1 Particle size*

114 Particle size distributions and mean particle diameter were measured using a Beckman Coulter
115 LS Series Laser Diffraction Particle Size Analyser; the data presented in Table 1 is the average
116 of triplicate runs.

117

118 *2.2.2 Total carbon content*

119 Total carbon content of samples was measured using a SKALAR Primacs Solid Sample TOC
120 Analyzer. Bulk samples were ground to < 250 µm using a mortar and pestle and three replicates
121 each weighing approximately 1000 mg were measured for total carbon by combustion at 1050
122 °C. Previous work with NL and UKC soils has shown the inorganic carbon content to be
123 negligible and total carbon content to be organic in origin (Doerr et al., 2005). Previous work
124 using soils obtained from a similar Nicholaston location to that of NIC1 and NIC2 soils,
125 recorded 27% inorganic carbon as part of the total carbon present (Personal communication,

126 Hallin, 2019), and the shape of the peak detection curves for total carbon analysis indicated an
127 inorganic carbon contribution of $\leq \sim 30\%$ for NIC1 and NIC2 soils, and $\leq \sim 10\%$ for LLAN1
128 soils.

129

130 *2.2.3 Drop shape and penetration imaging using Goniometer measurements*

131 Time-lapse images of the complete infiltration of a dispensed, detached water drop over time
132 were obtained using a KRUSS Easydrop FM40 goniometer. A 1000 μl syringe was set up to
133 dispense a drop of chosen volume (20, 50, 80 or 100 μl) at a rate of 200 $\mu\text{l min}^{-1}$. Images were
134 collected every 3-6 seconds depending on the rate of penetration and water repellency of the
135 soil being studied. Contact angles were obtained using Drop Shape Analysis (DSA) software
136 and a polynomial method was selected as the most appropriate for measurements as it can adapt
137 to a range of contour shapes at the three-phase contact.

138 The volume of water remaining on the soil as the drop penetrated was calculated as follows.
139 Fifteen image frames were selected at equal time intervals chosen to cover the penetration
140 process. These were converted into negative images in IrfanView (www.irfanview.com) and
141 enlarged and printed to approximately A4 size on 1 mm graph paper for measurement, using
142 the width of the goniometer syringe tip, measured using electronic callipers, as a 'scale bar' for
143 calibration. The drop volume remaining was calculated by splitting the drop printed image into
144 2 mm high segments and the lengths for each were recorded to the nearest mm. The volume
145 for each of these cylindrical segments was calculated and the volume of individual segments
146 summed to give the drop volume. As soil grains cover the surface of the water drop, the drop
147 will sit slightly lower than the initial soil surface in the small crater created from the movement
148 of grains up and around the drop. Therefore, part of the drop volume is hidden from view and
149 the volume obtained by the method above is slightly less than the true volume of water
150 remaining on the soil. So a small correction, made by visually estimating the depth of the crater
151 from the shape of that part of the drop which was visible and calculating the volume therein
152 using the method above, was made to the data to correct for this hidden volume. This 'hidden
153 volume' was never more than 15 % of the total drop volume and then only for NIC2 soil which
154 is the least repellent and where water penetrates the soil rapidly; for the remaining soils the
155 hidden volume was $< 10\%$. The volume of the drop which had penetrated the soil was obtained
156 by subtracting the volume remaining from the initial volume.

157

158 *2.2.4 Time-lapse imaging of water drops penetrating soil*

159 A Wessex WSA1 optical microscope fitted with a Brunel Microscopes Ltd Eyecam Plus
160 camera eyepiece was used to take time-lapse images of water drops penetrating soil.

161

162 *2.2.5 Water Drop Penetration Time*

163 The Water Drop Penetration Time (WDPT) test, as described by Letey (1969) and later in depth
164 by Doerr (1998), with water repellency classifications based on those by Bisdom et al. (1993)
165 was used to characterise the water repellency of the soils. A constant temperature and relative
166 humidity room at 20-22 $^{\circ}\text{C}$ and relative humidity 40-52 % was used. Samples and solutions

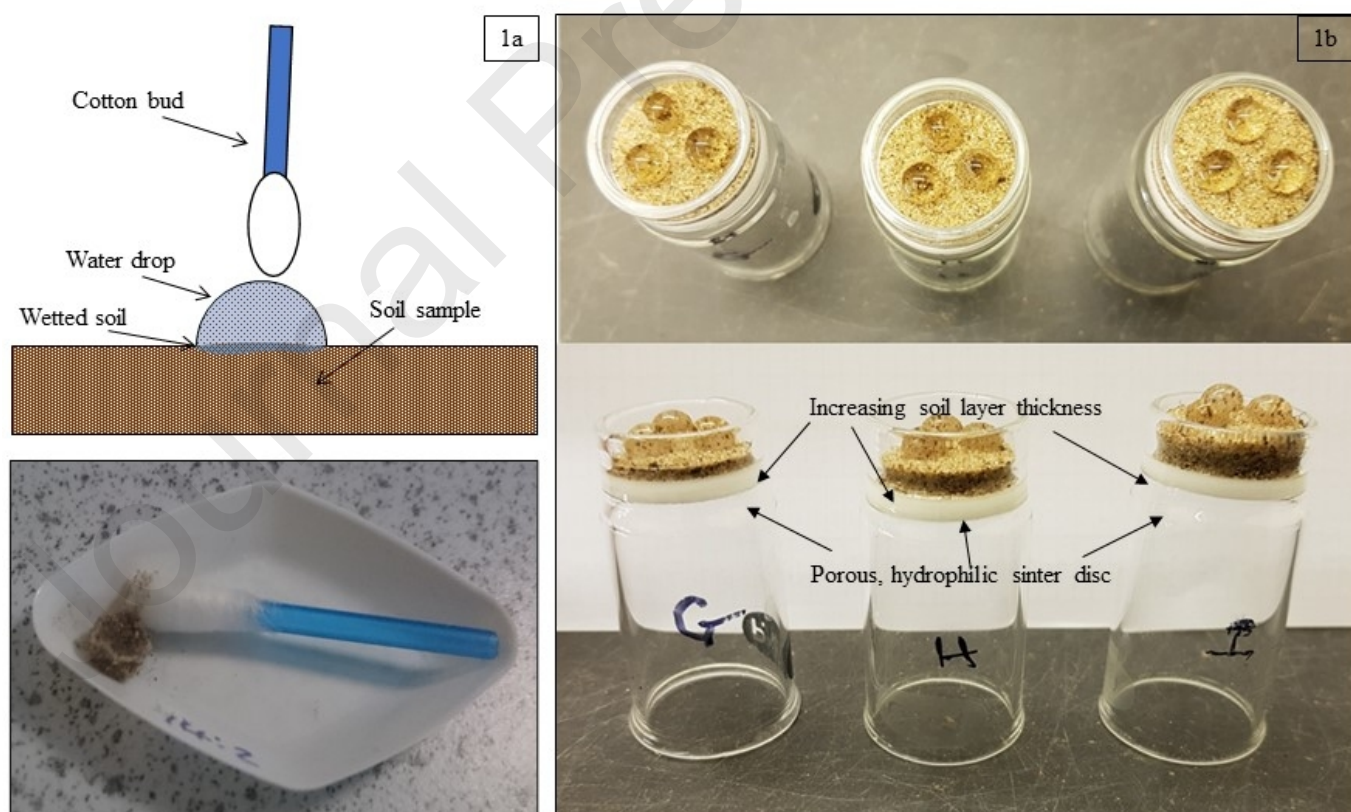
167 were left to equilibrate for a minimum of 24 hours prior to testing (Doerr et al., 2002). Soil
 168 samples were placed in plastic Petri dishes and gently tapped to create a level surface, with
 169 enough soil to allow sufficient depth for full penetration of drop. Six drops of distilled water
 170 of a given volume were dispensed on to the soil surface at timed intervals. Drops were
 171 dispensed from a height no greater than 5 mm to avoid soil displacement upon contact and the
 172 time from initial contact to full infiltration recorded.

173

174 2.2.6 Mass removal of soil grains over time – a ‘start-stop’ methodology

175 The aim of the experiment was to measure the mass of soil grains wetted at different intervals
 176 of penetration over time. Before experimentation samples were left to equilibrate for 48 hours
 177 in a controlled climate room at 20-22 °C and relative humidity 40-52 %. Each soil sample was
 178 placed on an analytical balance and the balance tared. The weight of the soil sample prior to
 179 each drop being dispensed on to the surface was recorded, followed by the weight immediately
 180 after, 6 drops were dispensed for each sample interval. For each soil tested a series of intervals
 181 were sampled based on the overall WDPT for that soil. For example, a soil with a 5-minute
 182 WDPT was sampled every 30 seconds, whereas a soil with a 15-minute WDPT was sampled
 183 every 60 seconds. After the appropriate time had elapsed, a pre-weighed cotton bud was
 184 brought into contact with the water drop and the water and soil grains that had been wetted
 185 adhered to the cotton bud and were removed for weighing (Figure 1a).

186



187 **Figure 1** Experimental set-up for (a) mass removal and (b) sinter based water drop penetration
 188 time studies. (a) Schematic of cotton bud being brought into contact with a water drop (top)
 189 and example of mass removed sample using the cotton bud method (bottom). (b) Image
 190 showing soils of varying thickness on top of a glass sinter disc.
 191

192

193 The method was easily reproduced, and the cotton bud was effective at removing the water
194 drop and attached wetted soil grains.

195

196 *2.2.7 Sinter based water drop penetration time through different thickness of soil*

197 In these experiments the soil was layered on top of a glass sinter disc (see Figure 1b). This
198 acted as a hydrophilic layer which presents a very low barrier to water penetration, and so the
199 time measured for infiltration gives a good approximation of the time for the water drop to
200 penetrate through the soil layer only. Different depths of soil, as determined by soil mass
201 distributed over the measured surface area of the sinter, were placed in 18-20 mm diameter
202 grade 3.0-4.0 (40-120 μm) glass sinter funnels and the time taken for water drops to infiltrate
203 the soil recorded. A constant temperature and relative humidity room at 20-22 $^{\circ}\text{C}$ and relative
204 humidity 40-52 % was used. The soil samples were weighed into small glass vials and placed
205 in the constant temperature-humidity room for 48 hrs prior to testing. Drops of 20, 30, 50 and
206 80 μl were used with a minimum of 3 drops for each depth tested.

207

208 *2.2.8 Loose- and settle-packed density*

209 Loose- and settle-packed bulk density measurements were made as follows. An empty,
210 stoppered, 10 ml glass volumetric flask was weighed. Soil was then added to the flask until
211 the sample reached the 10 ml line. The flask was then stoppered and the weight recorded, and
212 this weight was used to calculate the loose-packed density. Next the stopper was removed and
213 flask gently tapped, causing the soil to settle and pack more tightly, additional soil was then
214 added to the flask until it reached the 10 ml calibration line and no further tapping would create
215 any extra space. The sample was then re-weighed and the settle-packed density calculated.

216

217 *2.2.9 Profilometer*

218 UKC (wetttable) soil was sprinkled onto a square of adhesive tape attached to a glass
219 microscope slide. The slide was tapped to remove any loose grains and the process repeated
220 until a close packed covering of soil grains was achieved. Profilometer measurements of this
221 soil surface were made using a Dektak profilometer with a 12.5 μm stylus and a manual moving
222 platform. Profile data was collected over 10,000 μm lengths and at 25 μm spaced intervals.

223

224 *2.2.10 Dimensions of wetted soil pellets*

225 Dimensions of the soil pellets at different stages of water penetration, used liquid nitrogen to
226 freeze the water drops at different times of penetration, were obtained using AUC (wetttable)
227 soil, with the height and depth of the frozen pellet measured using electronic callipers. Soil
228 samples were placed into small glass vials and tapped gently to give a level surface. A water
229 drop was then dispensed onto the soil surface. At a set time the glass vial with sample was
230 carefully lowered into liquid nitrogen a left there for approximately 60 s. The frozen pellet was
231 turned out from the glass vial for measurement.

232

233 **3. Theoretical considerations**234 **3.1 First stage of soil water interactions: adhesional wetting**235 *3.1.1 Energy terms, total energy change, and depth of particle penetrating into the surface of*
236 *a water drop for a single spherical particle*

237 Consider the first stage of wetting in which a soil particle makes contact and is partially ‘taken
238 into’ a water drop, i.e. the drop and particle adhere, Figure 2. For simplicity, initially we ignore
239 any gravitation energy terms and assume a spherical particle for which the difference in
240 diameters between particle and drop is large enough that the drop can be considered flat across
241 the diameter of the particle, and that the increase in liquid-vapour interface of the drop arising
242 from the immersion of the particle in the drop is so small as to be negligible. (When the particle
243 enters the drop the increase in effective volume of the drop, i.e. drop volume plus volume of
244 particle inserted, increases the liquid-air interface; e.g. if a particle the same size as the drop
245 was completely inserted then the volume enclosed by the liquid surface would be twice the
246 original drop volume and the area of the liquid vapour interface would increase
247 commensurately).

248 The portion of the particle of radius r taken into the water drop to a penetration depth d (see
249 Figure 2a) is a spherical cap with area $2\pi rd$ (Wolfram Mathworld, 2019), and the change in
250 energy in making the solid-liquid surface formed is given by Eq. 1 below:

$$251 \quad \Delta G_{SL} = (\gamma^{SL} - \gamma^{SV})2\pi rd \quad (1)$$

252 where: ΔG_{SL} is the change in Gibbs energy of the solid-liquid(water) interface, γ^{SL} is the surface
253 tension of the solid-liquid(water) interface, γ^{SV} is the surface tension of the solid-vapour(air)
254 interface, r is the radius of the particle and d is the depth of penetration of the soil particle into
255 water.

256

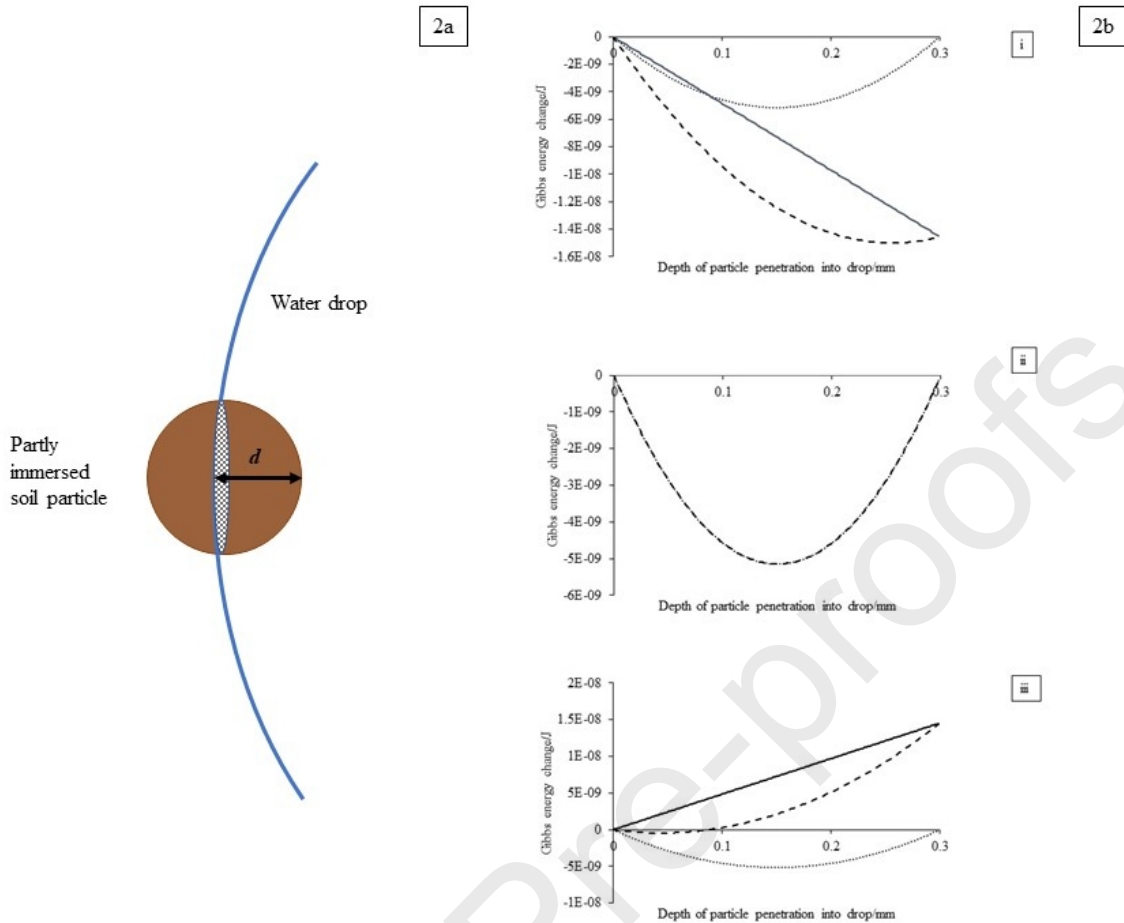
257 The area of the circle across the interface plane of the spherical cap (Wolfram Mathworld,
258 2019) and resultant change in energy from the loss of liquid-vapour surface area is given by
259 Eq. 2:

$$260 \quad \Delta G_{LV} = \gamma^{LV}(2rd - d^2) \quad (2)$$

261 where: ΔG_{LV} is the change in Gibbs energy of the liquid(water)-vapour(air) interface, γ^{LV} is the
262 surface tension of the liquid(water) -vapour (air) interface, r is the radius of the particle and d
263 is the depth of penetration of the soil particle into water.

264

265



266

267 **Figure 2** Gibbs energy change for the loss of liquid-vapour interface and increase of solid-
 268 liquid interface as a soil grain penetrates into the surface of a water drop for a single spherical
 269 particle. **a)** Wetting of a spherical particle as it is taken into a water drop to depth d . **b)** Gibbs
 270 energy change (J) for a single soil particle of 0.15 mm radius penetrating into a 100 μl drop
 271 (mm) during the wetting process, all with particle radius of 0.15mm and (i) where $\theta = 45^\circ$, (ii)
 272 where $\theta = 90^\circ$ and (iii) where $\theta = 135^\circ$. Where: the Gibbs energy change from the loss of
 273 liquid-vapour interface is given as a dotted line; the Gibbs energy change for the increase of
 274 solid-liquid interface is given as a solid line; and the overall Gibbs energy change
 275 (summation of previous two terms) is given as a dashed line. The particle will penetrate the
 276 water drop to the point where $(\partial G/\partial(\text{depth})) = 0$, i.e. the slope of the dashed line in the
 277 diagram is zero.

278 For this situation the Gibbs energy at any penetration depth, d , is given by the sum of two
 279 terms: the first term is associated with the increase in solid-liquid interface from the formation
 280 of the spherical cap and the second term is associated with the decrease in liquid-vapour
 281 interface which is equal to the area of the circle of the particle at the depth of contact. Figure
 282 2b shows both energy terms and their summation for a particle of 0.15 mm radius, and contact
 283 angles, (θ) , of 45 (i), 90 (ii) and 135° (iii) respectively. The particle will move into the drop
 284 until $(\partial G/\partial \text{depth}) = 0$, and so the depth to which the particle penetrates the drop is determined
 285 by the contact angle (θ) . For a particle with $\theta = 90^\circ$ taken into an infinitely large drop the
 286 particle penetrates up to the halfway point as this gives the greatest decrease in liquid-vapour
 287 surface area; for $0 < \theta < 90^\circ$ the particle penetrates further but is never fully covered; for $\theta >$
 288 90° the particle penetrates to a shallower depth; while for $\theta = 180^\circ$ it does not penetrate at all.

289

290 *3.1.2 Energy terms, total energy change, and depth of drop penetrating into the surface for a*
291 *hemisphere drop wetting a single layer of close-packed spheres*

292 The Gibbs energy change involved in the wetting of a single layer of particles can be estimated
293 for a hemisphere of water sitting on homogenous, close-packed, single sheet of spherical
294 particles using the following approximations.

295 1) The drop is a hemisphere and retains this shape throughout the wetting process. The choice
296 of a hemisphere for all soils is a convenience, it allows comparisons for equal area of water/soil
297 contact for all soils. We recognise that strongly water repellent soils have a smaller initial
298 contact area than less water repellent soils (see Figure 5) (Balshaw, 2019), but the interfacial
299 interactions, which are the major energetic factors involved, all vary linearly with contact area.
300 Hence the shapes of the energy curves in Figure 5 will remain essentially the same irrespective
301 of contact area, only the absolute values of the energies involved i.e. the scale of the y axis in
302 Figure 5 will vary. No allowance is made for the increased surface area of the drop due to
303 changes in the curvature of the surface upon contact with the soil.

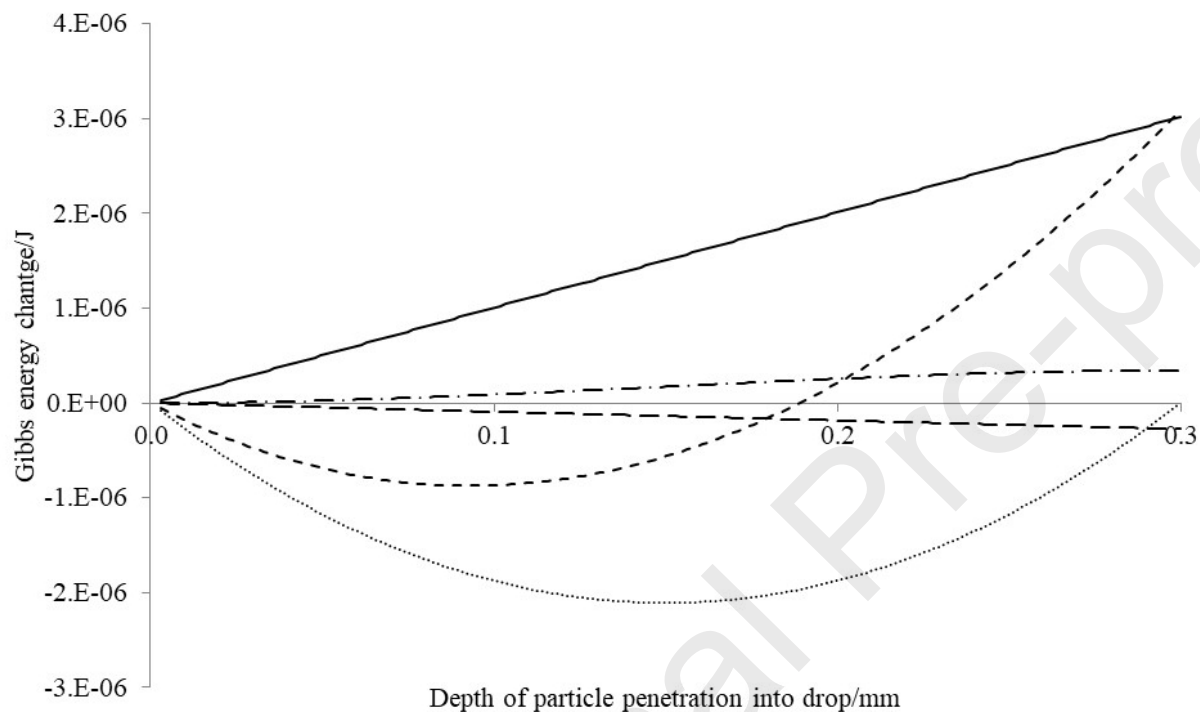
304 2) The soil is made up of uniform, smooth, spherical particles with a packing density of close-
305 packed spheres (Chang and Wang, 2010).

306 3) As the drop moves over the particles in this initial stage it does so with no lateral spread,
307 and when accounting for gravitational energy (which is only a small contributor to the overall
308 energy) the centre of mass of the hemisphere moves by the depth of penetration even though
309 the particles will occupy some of the volume of the base of the hemisphere.

310 4) The increase in volume of the hemispherical drop as soil grains penetrate into the hemisphere
311 causes an increase in the liquid-vapour surface area. This is a relatively small factor, and we
312 estimate this from the surface area of a hemisphere composed of liquid plus volume of particles
313 penetrating the liquid.

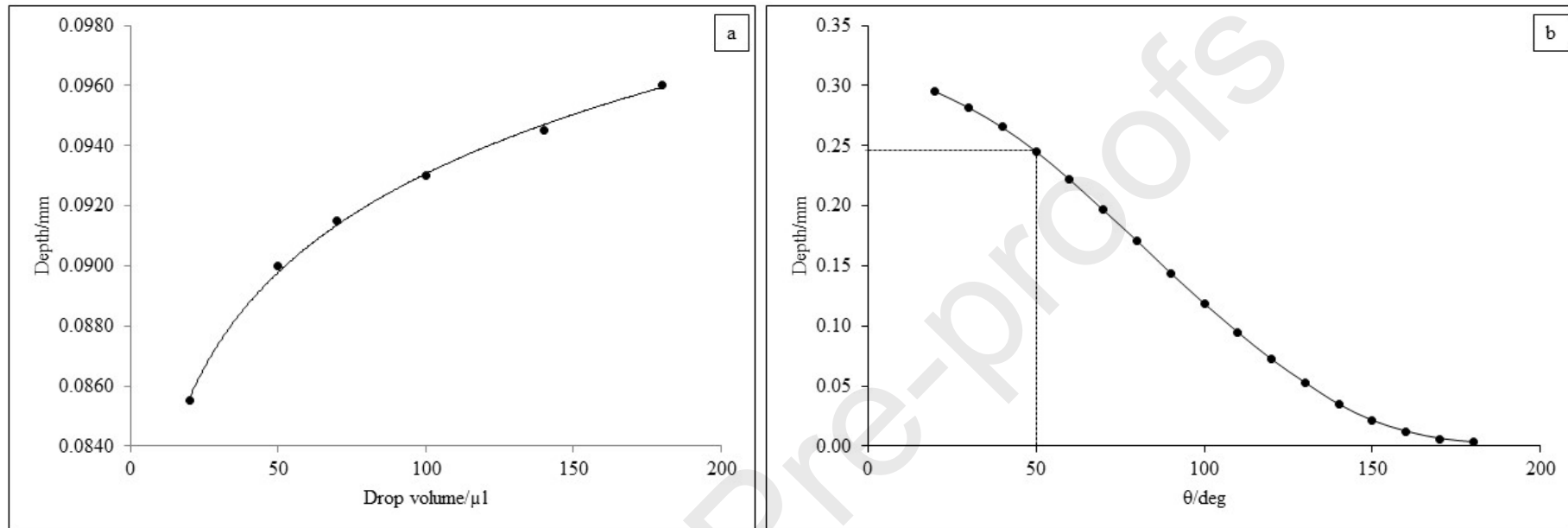
314 Figure 3 gives diagrams for a representative example of particles with radius 0.15 mm and drop
315 volume of 100 μl with a wax coating with contact angle of 111° , which corresponds to that for
316 paraffin wax. Note that the relatively small energy contributions from gravity and the
317 increasing total volume as particles penetrate the drop work in opposite directions, and thus
318 effectively cancel one another out. Also, while gravity is not a major energy term it does have
319 some influence on the depths to which water drops of different volumes will sit on the soil
320 grains, with larger drops settling slightly deeper into the soil as shown in Figure 4a.

321 While soil is not a collection of close-packed identical spherical particles, the general ideas of
322 the competing energy terms considered here, general patterns of behaviour, and their
323 dependence on surface contact angle, give a useful insight into the initial water soil interactions
324 following contact between a water drop and real soil.



326

327 **Figure 3** Gibbs energy change (J) for a single sheet of close-packed particles, with depth of particle penetration into the drop (mm) during the
 328 wetting process, where $\theta = 111^\circ$, drop volume and particle radius of 0.15 mm for drop size 100 μl showing the gravity term as a long dash. Where:
 329 the Gibbs energy gained from the loss of liquid-vapour interface is given as a dotted line; the Gibbs energy gained by the increase of solid-liquid
 330 interface is given as a solid line and the overall Gibbs energy (summation of terms) is given as a dashed line.



331

332 **Figure 4** Dependence of the depth of water drop penetration upon (a) drop volume and (b) contact angle for a water drop on close-packed spheres.
 333 **a)** Depth of the water drop on close-packed spheric particles of 0.15 mm radius against drop volume for $\theta = 111^\circ$ (the contact angle for paraffin
 334 wax on a flat surface). **b)** Depth of water penetration against soil contact angle (θ) for 100 μl drop on 0.3 mm diameter particles (The dashed lined
 335 shows the $0.15 \times 1.63r$ (0.245 mm) penetration depth, and corresponding theta of 50 degrees).

336

337 Kinetically, adhesional wetting to a surface of unchanging θ is very rapid. On the time scales
338 of our experiments it is essentially instantaneous as soil and water make contact.

339

340 **3.2. Second stage of soil water interaction: the transition from adhesion to infiltration**

341 The next step in the process must involve the water drop penetrating through the first layer of
342 soil particles adhering to it into the second and subsequent layers.

343 Previous research (Douglas et al., 2007; Diehl and Schaumann, 2007) has suggested for
344 spreading wetting to occur in water repellent soils, the non-polar organics present on the surface
345 of the soil grains will have to undergo chemical changes or reorientation of molecules to permit
346 the penetration of the water wetting front into the soil profile. The rate (change in area wetted
347 per unit time) for the wetting of a surface undergoing such a change will depend on two factors:
348 1) the rate constant for the rearrangement of the surface molecules, and 2) the length of the
349 contact front between soil and water, i.e.

$$350 \text{Rate} = kL_{CF(t)} \quad (3)$$

351 Where k is the rate constant for wetting, and $L_{CF(t)}$ is the length of the contact front at time t ;

352 and k is a rate constant of the usual form.

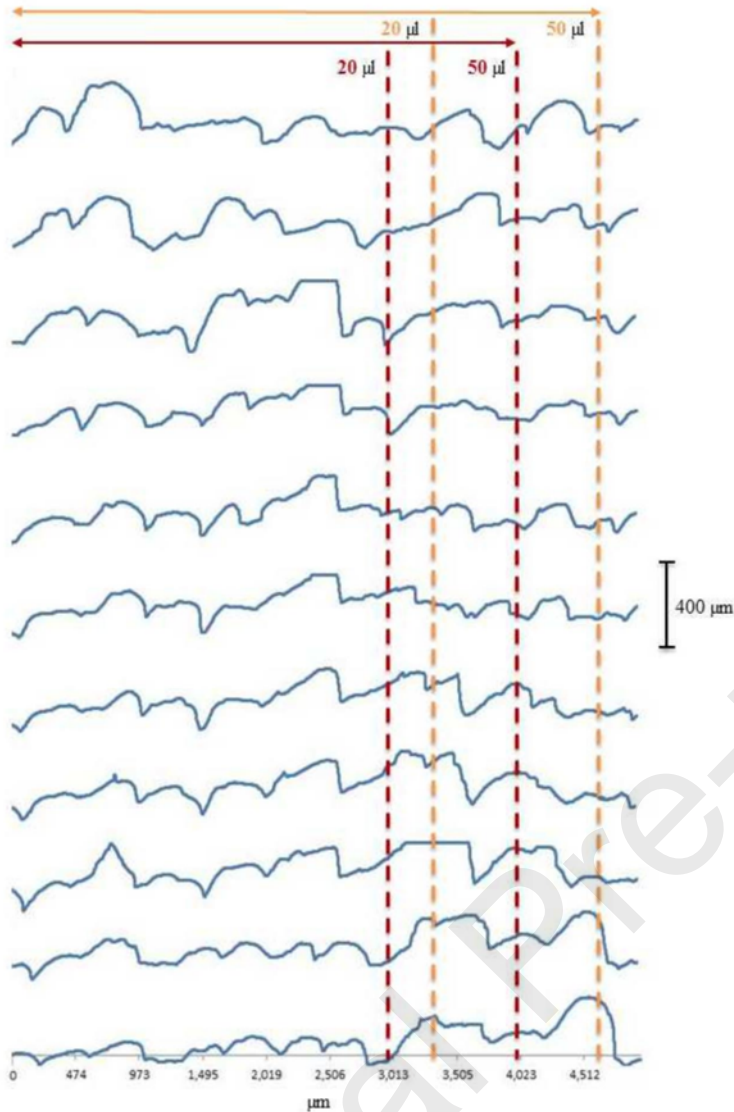
$$353 k = Ae^{(-E_{act}/RT)} \quad (4)$$

354 Where A is the pre-exponential factor, E_{act} the activation energy, R , the Gas Constant, and T
355 temperature in Kelvin. The relatively low activation energies measured for soil wetting indicate
356 that the surface reorganisational processes involved are physical in nature rather than the
357 breaking of chemical bonds (Diehl and Schaumann, 2007; Balshaw, 2019). Because of the way
358 the drop sits on the soil, the initial contact length, $L_{CF(t)}$ when $t=0$, will be smaller the more
359 water repellent the soil, all other things being equal.

360 The transition from adhesional wetting to branching interstitial wetting occurs as the drop
361 covers the soil particles from initial contact sufficient to reach a depth over the first contact
362 layer to allow access to the surface of particles below this layer. Shirtcliffe et al. (2006) give
363 this depth, for close packed spheres of radius r , as $2(2/3)^{1/2}r$ (i.e. $1.63r$) and, using a geometric
364 approach to determine free energy changes, they calculate a contact angle of 50.73° to reach
365 this depth. The depth of water penetration against contact angle for 100 μl drop using the
366 energetic approach given here is shown in Figure 4b, from which a critical contact angle to
367 reach this depth of 0.245 mm is calculated to be 50° which is in good agreement with that
368 calculated by Shirtcliffe et al. (2006).

369 Based on the calculation assumptions underlying Figure 4b for spherical, homogenous, close-
370 packed, spheres a critical contact angle of $\leq \sim 50^\circ$ (identified as $\theta_{critical}$ in the following
371 discussion) would be necessary for the water to make immediate contact with the second layer
372 of spheres. However, soil is not made up of particles which are uniform in size and shape, nor
373 are they necessarily close-packed. Some idea of the surface characteristic of natural soil, is
374 given by the surface profile of a layer adhering to a strip of adhesive tape shown in Figure 5.

375

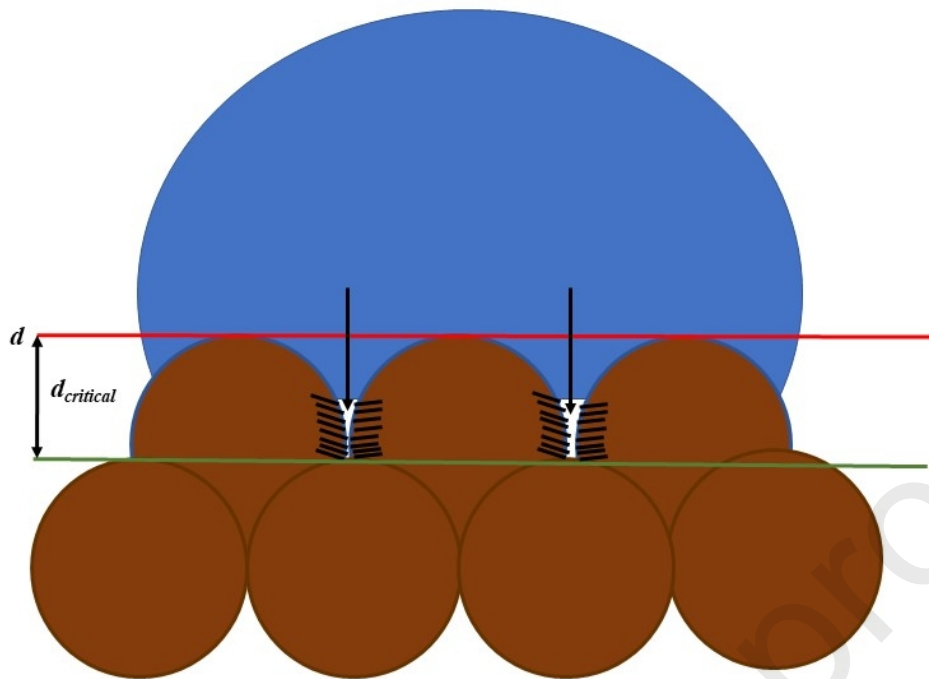


376

377 **Figure 5.** Cross-sectional profiles from profilometer measurements on UKC soil showing
 378 surface roughness; 10 mm long scans at 25 μm spaced intervals, with 400 μm vertical scale
 379 marker shown. Approximate diameters of the contact circles for 20 and 50 μl drop on NIC2
 380 (orange) which is a strongly repellent soil, and NL1 (red) which is a severely-extremely
 381 repellent soils, obtained from goniometer images, are also shown.

382

383 In a loose- or settled-packed arrangement with a distribution of particle sizes there will be local
 384 variations in distances between first and second soil layers, leading to a distribution of such
 385 distances beneath a water drop. While the precise nature of this distribution will determine the
 386 overall rate of contact with the second layer of soil particles, the smaller of the distances will
 387 be the most critical, thus θ_{critical} for a natural soil is expected to be larger, perhaps significantly
 388 larger depending on particle size and shape distribution, than 50° . Whatever the actually value
 389 of θ_{critical} , in a water repellent soil with $\theta > \theta_{\text{critical}}$, a reduction of the initial contact angle to θ_{critical} ,
 390 thought to be associated with molecular restructuring, is required to allow water contact to
 391 move from the first contact layer into the second layer, and then into bulk soil, as illustrated
 392 schematically in Figure 6.



393

394 **Figure 6.** Schematic of water drop sitting on soil grains. Branching interstitial wetting and
 395 penetration into bulk soil cannot occur until hatched area undergoes a change in hydrophobicity
 396 to permit water flow. The movement of water from the depth from where the water drop is
 397 initially sitting on the grains to the critical depth where it reaches the second layer of grains is
 398 controlled by this change in θ to $\theta_{critical}$.

399

400 3.3. Third stage of soil water interaction: penetration into bulk soil

401 3.3.1 Theoretical considerations

402 A kinetic model for water moving through a uniform array of uniform spheres could be built
 403 around uniform sequential vertical movement through subsequent layers, with movement from
 404 each layer to the next inhibited by the same need to match a constant $\theta_{critical}$ (Shirtcliffe et al.
 405 2006), however, for a natural soil, with a distribution of particle sizes, shapes, and probably
 406 surface hydrophobicities, the regularity of the array, and with it regularity of water movement,
 407 is lost within a relatively short distance. So, once water penetrates into bulk soil, filling of
 408 vacant soil interstices is not limited to vertical flow only, can occur from many directions, and
 409 is expected to lead to lateral spreading of wetting. Furthermore, since routes which are fastest
 410 i.e. those involving the largest local $\theta_{critical}$, will dominate the process, then the degree of
 411 molecular rearrangement required for interstitial wetting is probably less demanding than that
 412 required for wetting to extend from the first to second soil layers.

413 Since water moves in between soil particles and wets them in interstitial wetting there is no
 414 change in the liquid-vapour area, therefore, the overall Gibbs energy change for this process,
 415 ΔG_s is given as (Equation 5):

$$416 \quad \Delta G_s = \Delta_{area}(\gamma^{SL} - \gamma^{SV}) \quad (5)$$

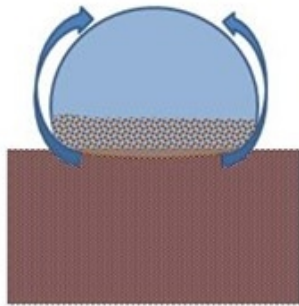
417 where: ΔG_s is the change in Gibbs energy for interstitial wetting, Δ_{area} the change in area
 418 wetted, γ^{SL} is the surface tension at the solid-liquid(water) interface and γ^{SV} is the surface
 419 tension at the solid-vapour(air) interface.

420 From energetic considerations alone, interstitial wetting can occur for any contact angle where
 421 $\theta < 90^\circ$ and will not occur for $\theta > 90^\circ$ so, irrespective of $\theta_{critical}$, for cases where $\theta > 90^\circ$,
 422 molecular rearrangement of surface molecules along the contact front is required before
 423 penetration can occur.

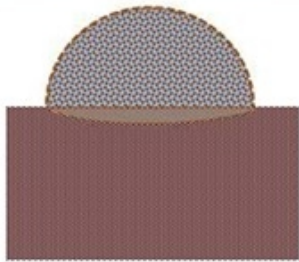
424

425 Consider the scenario where $\theta \leq \theta_{critical}$. Here rapid infiltration through the first layer of soil
 426 particles around the drop would be expected, followed by rapid branching interstitial wetting
 427 through the pores of the soil; water penetration would be seen as a single continuous process.
 428 However, if $\theta > \theta_{critical}$ rapid infiltration cannot occur, therefore the transition from adhesional
 429 wetting to interstitial wetting requires some change in the chemical nature of the solid-liquid
 430 interface i.e. molecular restructuring. We might then expect to be able to see the separate stages
 431 of water penetration experimentally: i.e. a rapid initial adhesional wetting, followed by an
 432 induction period while molecular reorganisation occurs before movement of water beyond the
 433 first layer of wetted particles into the second layer of particles can occur, and then the
 434 accelerating process of branching interstitial wetting, as the water drop penetrates into the soil.
 435 Figure 7 gives a schematic summary of the proposed process.

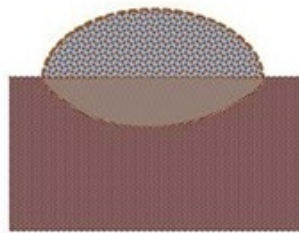
436



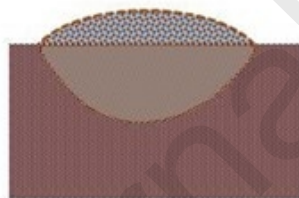
Adhesion-immersional wetting is the initial stage where water drop is dispensed onto soil surface and grains are forced up and around the water drop. The liquid-vapour interface is reduced by adhesional wetting of soil grains, leading to a layer of packed grains around the drop.



Adhesional wetting continues as the water drop becomes fully (as shown) or partially covered by a loose-packed layer of soil grains. Due to removal of grains up around the drop a small crater is formed underneath the water drop.



A molecular reorganisation on the surface of soil particles at the water/air/solid contact line reduces θ to $\theta_{critical}$ such that branching interstitial wetting commences through the first layer of adhering grains in the bulk soil.



As branching interstitial wetting continues to increase the wetting contact line the rate of interstitial wetting accelerates.



Full penetration of water drop into soil.

437

438 **Figure 7.** Schematic showing the proposed wetting processes in a water repellent soil.

439

440 **4. Experimental results and discussion**

441 *4.1. Soil characterisation*

442 Table 1 gives soil source locations and physical characteristics. To aid the reader, in
443 subsequent discussion water repellency class is given in parentheses after the soil name
444 where useful.

445

Journal Pre-proofs

446 **Table 1** Source locations and soil characterisation of the soils used.

Code	Country	Site location, Region	Lat/Long	Vegetation type	Sample depth (cm)	Mean diameter (mm)	Total carbon content (g kg ⁻¹)	Water repellency class*	Bulk density loose-packed (g cm ⁻³)	Bulk density settle-packed (g cm ⁻³)	Mean particle diameter (µm)	Fractional void space	Average total carbon (Wt %)
UKC	Wales	Nicholaston, Gower	51°35'N 04°06'W	N/A – bare dune	0.10	0.39	^a 2.5 ±0.5	Wettable	-	-	435.3 ±3.5	-	-
AUC	Australia	Pine Views, Naracoorte	36°30'S 140°42'E	Cropland	0-10	0.24	^b 2.2 ±0.4	Wettable	-	-	-	-	-
NIC2	Wales	Nicholaston, Gower	51°34'N 4°7'W	Dune grass	0-10	0.33	^c 6.7 ±0.7	Strongly	1.443	1.598	334.9 ±1.8	0.397	0.67 ±0.07
LLAN1	Wales	Llanmadoc, Gower	51°37'N 4°15'W	Pine forest	0-10	0.27	^d 21.9 ±4.4	Strongly	1.208	1.459	274.0 ±0.3	0.450	2.19 ±0.44
NIC1	Wales	Nicholaston, Gower	51°34'N 4°7'W	Dune grass	0-10	0.32	^c 4.5 ±0.3	Severely	1.418	1.603	322.7 ±0.5	0.395	0.45 ±0.03
NL1	Netherlands	Zuid Holland, Ouddorp	51°48'N 03°54'W	Grass/moss	0.10	0.27	^a 5.1 ±1.1	Severely-extremely	1.184	1.405	286.9 ±4.4	0.470	0.33

447 ^a Previous work using soils obtained from a similar Nicholaston location recorded 27% inorganic carbon as part of the total carbon present (Personal communication, Hallin,
448 2019). In this work the shape of the peak detection curves for total carbon analysis indicates an inorganic carbon contribution of ≤~20%.

449 ^b Previous work by Doerr et al. (2005)

450 ^c In this work an assessment of the detection curves for Llanmadoc soils indicates a contribution of ≤~20%.

451 ^d In this work an assessment of the detection curves for Llanmadoc soils indicates a contribution of ≤~10 %.

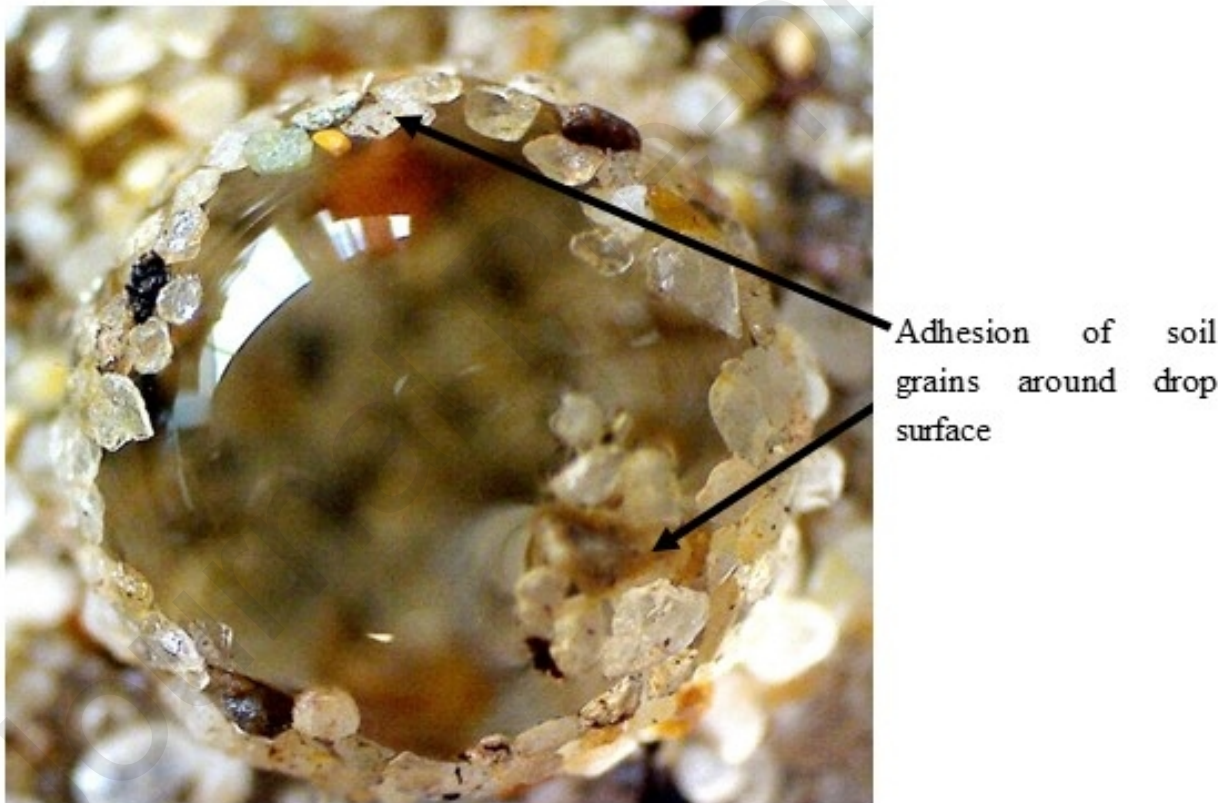
452 *Determined from WDPT test and classification of Bisdom et al. (1993)

453

454 4.2 Optical microscopy and time-lapse images

455 Optical microscopy provides visual confirmation of the initial adhesional wetting stage in water
 456 repellent soils, as shown in Figure 8 for NIC1 (severely) soil. where loosely packed soil
 457 particles can be seen adhered to, and partly taken in to, the water drop. Over time soil particles
 458 are observed jostling underneath the water drop, which results in them being forced up and
 459 around the drop. During this process it appears that the drop begins to penetrate into the soil,
 460 but, initially at least, this is due to the drop sitting lower than the initial soil surface in the small
 461 crater that has formed as soil particles are displaced upwards from underneath the drop. During
 462 the WDPT tests it was observed that this process occurred at different rates depending on the
 463 severity of the water repellency of the soil. For example, a layer of soil particles covered the
 464 drop on the lesser water repellent NIC2 (strongly) and LLAN1 (strongly) soils much more
 465 rapidly than for the high repellency NIC1 (severely) and NL1 (severely-extremely) soils. It is
 466 worth noting that for NL1 a full coverage of the drop with soil particles often did not occur
 467 before the drop began to infiltrate into the soil.

468



469

470 **Figure 8.** Optical microscopy image of water drop (20 μ l) on NIC1 soil showing the adhesional
 471 stage of wetting process with grains adhered to the drop surface.

472

473 It is the forces of surface tension which drive the movement of soil particles from underneath
 474 the drop and allows them to jostle and move such that the drop is covered by as many accessible
 475 particles as is energetically and kinetically possible. As soil particles adhere to the drop surface

476 it causes a loss in water-vapour interface which is replaced by the creation of a soil-water
 477 interface. Calculations of the energetics of this process indicate that the energy released
 478 through the destruction and formation of these interfaces is enough to lift soil particles (of the
 479 sizes found in soils used here) to the top of a 100 μl drop, although this does not include any
 480 consideration of inter-particulate or particle-water friction inhibiting movement.

481 We note an interesting asymmetry in the behaviour of soil particles adhering to the drop on the
 482 top of the drop and those beneath; those on the top do not end up being completely wetted and
 483 taken into the drop whereas those at the bottom do. Soil particles on top of the drop almost
 484 always remain in place adhering to the drop until they are deposited onto the soil surface when
 485 the drop penetrates completely into the soil. This is because to completely wet the particles on
 486 the top of the drop requires the reformation of the relatively high energy water-vapour interface
 487 over the particle, whereas for particles at the bottom what is formed is a new liquid-solid
 488 interface at the next layer of particles and there is no increase in water-vapour interface. So,
 489 the asymmetry is not so much between particles adhering to the top or bottom of the drop, but
 490 rather one between particles which have no adjacent contacting layers of particles and ones that
 491 do.

492

493 *4.3 Initial mass pick up (mass removal experiments)*

494 The masses of soil particles adhering to the drop after ~ 8 seconds contact, are given in Table
 495 2.

496 **Table 2.** Initial mass of soil wetted (within 8 s) per soil type and drop volume

Drop volume (μl)	Mass wetted (g)			
	NIC2 (Strongly)	LLAN1 (Strongly)	NIC1 (Severely)	NL1 (Severely- extremely)
20	0.0175	0.0152	0.0155	0.0052
50	0.0516	0.0176	0.0242	0.0078
80	0.0450	0.0225	0.0276	0.0118
100	0.0729	0.0354	0.0374	0.0158

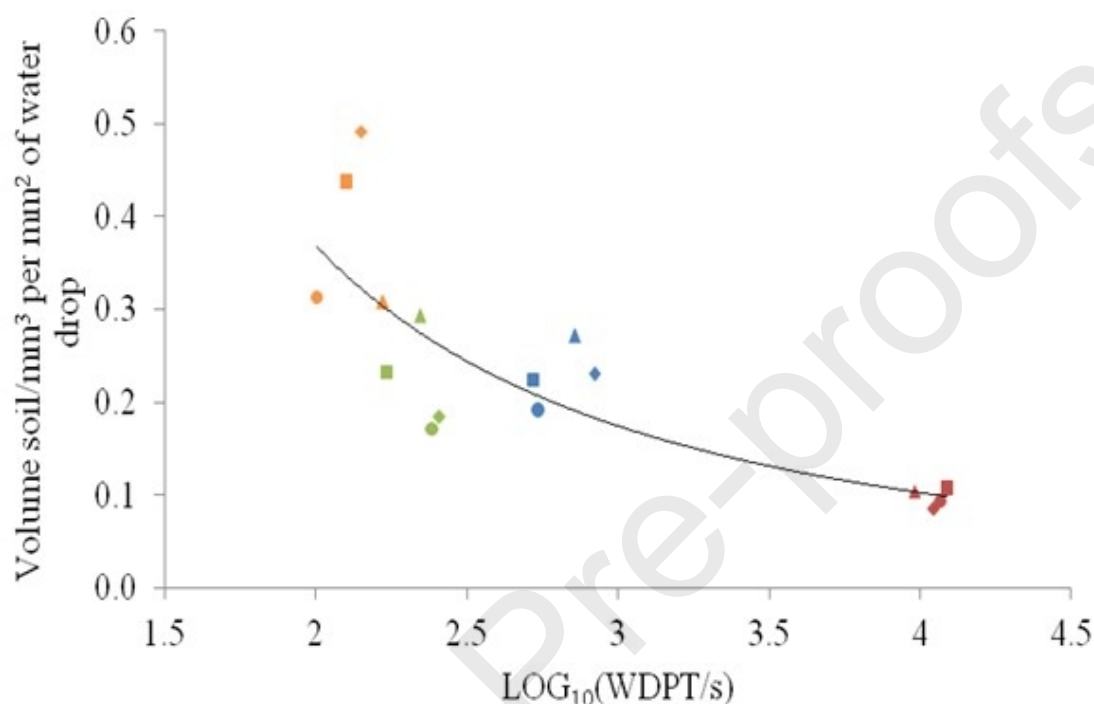
497

498

499

500 Using these and soil packed-density data we can estimate the volume of soil adhering per unit
 501 surface area of the drop, and these values are plotted against $\log_{10}(\text{WDPT}/s)$ in Figure 9 (the
 502 choice of a log scale for WDPT is for convenience only, it has no theoretical significance).

503



504

505 **Figure 9.** Initial volume of soil (mm^3) per mm^2 of water drop against log water drop penetration
 506 time for NIC2 (strongly) (orange) and LLAN1 (strongly) (green) NIC1 (severely) (blue), and
 507 NL1 (severely–extremely) (red). Triangle ($20 \mu\text{l}$), diamond ($50 \mu\text{l}$), circle ($80 \mu\text{l}$) square (100
 508 μl) soils at different drop volumes. The curve has been included just as a guide for the eye.

509

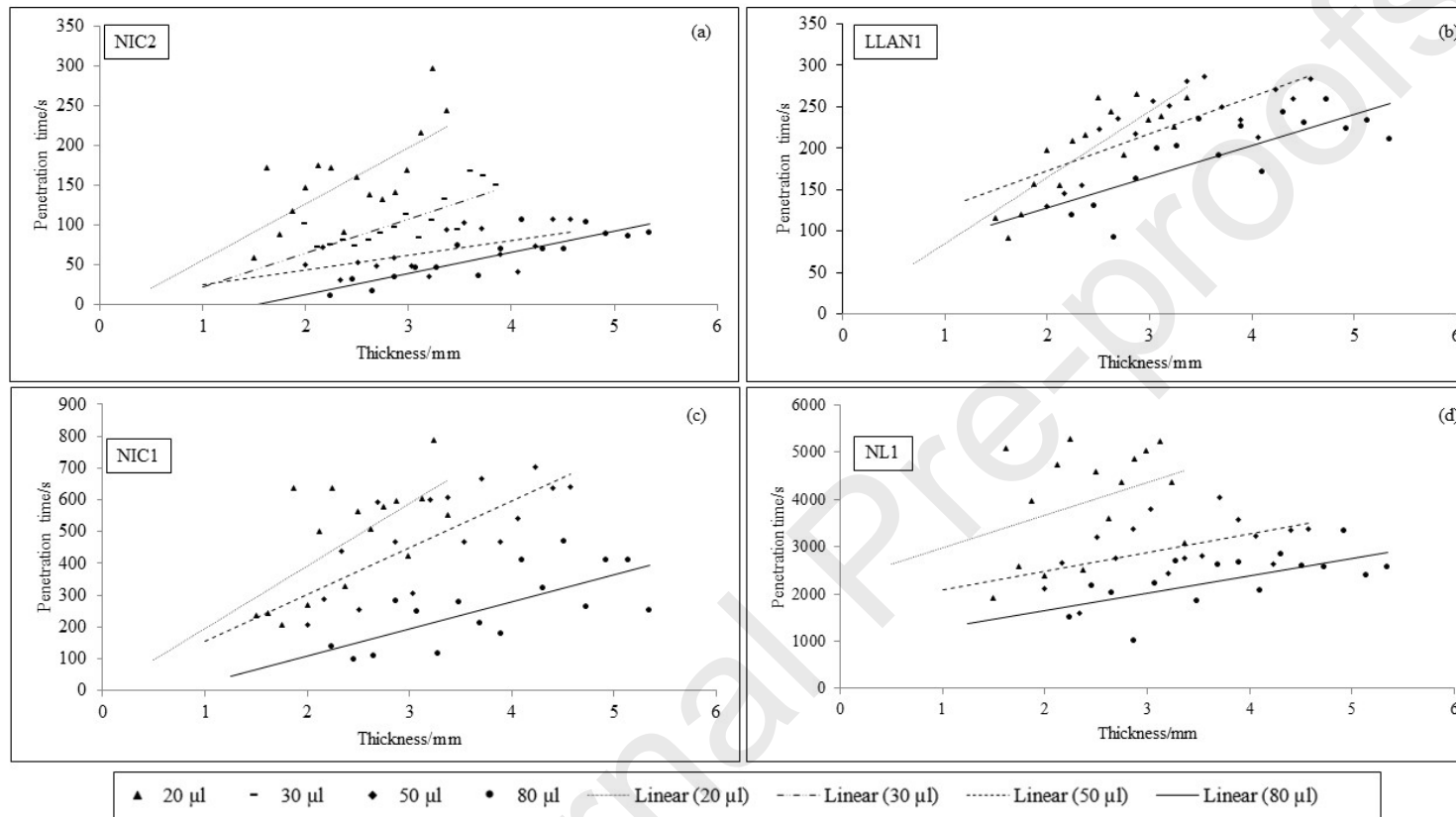
510 The data show that for the least repellent soil (NIC2, strongly), there is a 3-4 times greater
 511 volume of soil taken up per unit surface area of the water drop, compared to the most repellent
 512 soil (NL1, severely-extremely). The data here reflects observations made during the WDPT
 513 tests whereby soil particles are picked up and cover a water drop more rapidly for a less
 514 repellent soil compared to a more repellent one. This can be explained by the polarity of the
 515 soil surface and the relevant surface energies involved (Jaycock and Parfitt, 1981; Rigby et al.,
 516 1986); a less repellent soil will have a more polar surface compared to a more repellent soil
 517 and therefore more energy is released in the exchange of interfaces as solid and liquid surfaces
 518 come into contact for a less repellent soil than a more repellent soil.

519 4.4 Water drop penetration time through layers of soil of different thicknesses

520 If the concept of a multistage process with a kinetic barrier to the transition from adhesional
 521 wetting to branching interstitial wetting is correct then, in its simplest form, a plot of time taken
 522 to penetrate against thickness of soil should result in a positive intercept corresponding to the

523 time required for the kinetic barrier to be overcome, i.e. the data should show an induction
524 period. Figure 10 shows such plots for the four soils studied, obtained from drop penetration
525 times through different thickness of soil on sinters.

Journal Pre-proofs



527

528 **Figure 10.** Global plot of sinter water drop penetration time data, based on an average measurement from three drops per data point. **(a)** NIC2 **(b)**
 529 LLAN1 **(c)** NIC2 **(d)** NL1. Where, 20 µl is a triangle and corresponding linear line is dotted, 30 µl is a dash and corresponding linear line is dash
 530 dot dot, 50 µl is a diamond and corresponding linear line is dash and 80 µl is a circle and corresponding linear line is solid.

531 The data are quite scattered, and a number of equations of varying complexity give comparable
 532 correlation coefficients, but a linear fit is simple, and, for this data, gives as good a fit as any
 533 other equation. We propose then a relationship between overall penetration time, t_{pen} , and
 534 thickness of soil, T_{soil} , of the form:

$$535 \quad t_{pen} = t_{inf} + t_t T_{soil} \quad (6)$$

536 Where t_{inf} is the time between first contact and branching interstitial wetting to start i.e. the
 537 induction period, and t_t is the time taken to penetrate a fixed thickness of soil by branching
 538 interstitial wetting.

539 The most obvious observation to be drawn from Figure 10 is that overall penetration times for
 540 all soil thicknesses increase as drop volume decreases, but resolving this to show the
 541 dependence upon t_{inf} and t_t , i.e. intercept and slope in Figure 10, is difficult because of the
 542 scatter in the data. Only for the most repellent soil, NL1 (severely-extremely), do the data show
 543 a clear positive intercept (which increases as drop volume decreases). For the rest, intercepts
 544 are scattered around zero, and the high experimental errors in intercept determination prevent
 545 any definite conclusions to be drawn for these soils. We note however, an experimental
 546 complication to consider, in that the movement of soil grains from underneath the drop also
 547 causes the drop to move through the soil layer, although this is by displacement not penetration,
 548 , and the effect of this is to reduce the thickness of the soil layer the drop must penetrate to
 549 contact the sinter. We have made no correction for this for the data shown in Fig. 10, but if
 550 such a correction could be reliably applied the effect would be to reduce the x- axis value of
 551 each point on any given plot by the same fixed amount. This would lead to an increase in the
 552 intercept for each plot but leave the slope unchanged, and this means that all intercepts in Table
 553 3 are systematically low to some extent. Interpreting the variation in time to penetrate a fixed
 554 thickness of soil, t_t , (which is the inverse of rate of penetration), is also difficult because of the
 555 scatter in the data, but we note that for all soils t_t for 20 μ l drops is greater than that for larger
 556 drop volumes.

557 However, for the highly repellent soil, NL1 (severely-extremely), the data does show
 558 experimental resolution of the stages in the wetting of the soil. For NL1 both the intercept, i.e.
 559 induction period, and slope, i.e. time for interstitial wetting through a given thickness of soil,
 560 increase as drop volume decreases.

561 From the data on different drop volumes, we suggest the gravitation energy term may play
 562 some part in determining the rate of interstitial wetting for all soils studied. And we suggest
 563 the gravitation energy term may also influence the rate of transition from adhesional to
 564 interstitial wetting, at least for the most repellent soil studied.

565

566 **Table 3.** Intercepts and slope – sinter data.

Soil	Drop volume/ μ l	Intercept (s)*	Slope (s mm ⁻¹)*
NIC2	20	-17 \pm 35	72 \pm 14

	50	2 ±15	19 ±4
	80	-34 ±13	25 ±3
LLAN1	20	38 ±28	62 ±11
	50	99 ±36	42 ±11
	80	14 ±27	45 ±7
NIC1	20	-25 ±110	210 ±42
	50	-12 ±89	151 ±27
	80	-111 ±65	94 ±17
NL1	20	2442 ±667	610 ±256
	50	1679 ±442	397 ±134
	80	656 ±295	421 ±79

567 *Error estimate is one standard deviation

568

569 *4.5 Time-dependent measurements of contact angle, volume of water penetrated, mass of soil*
 570 *wetted, and size of water/wetted-soil pellet*

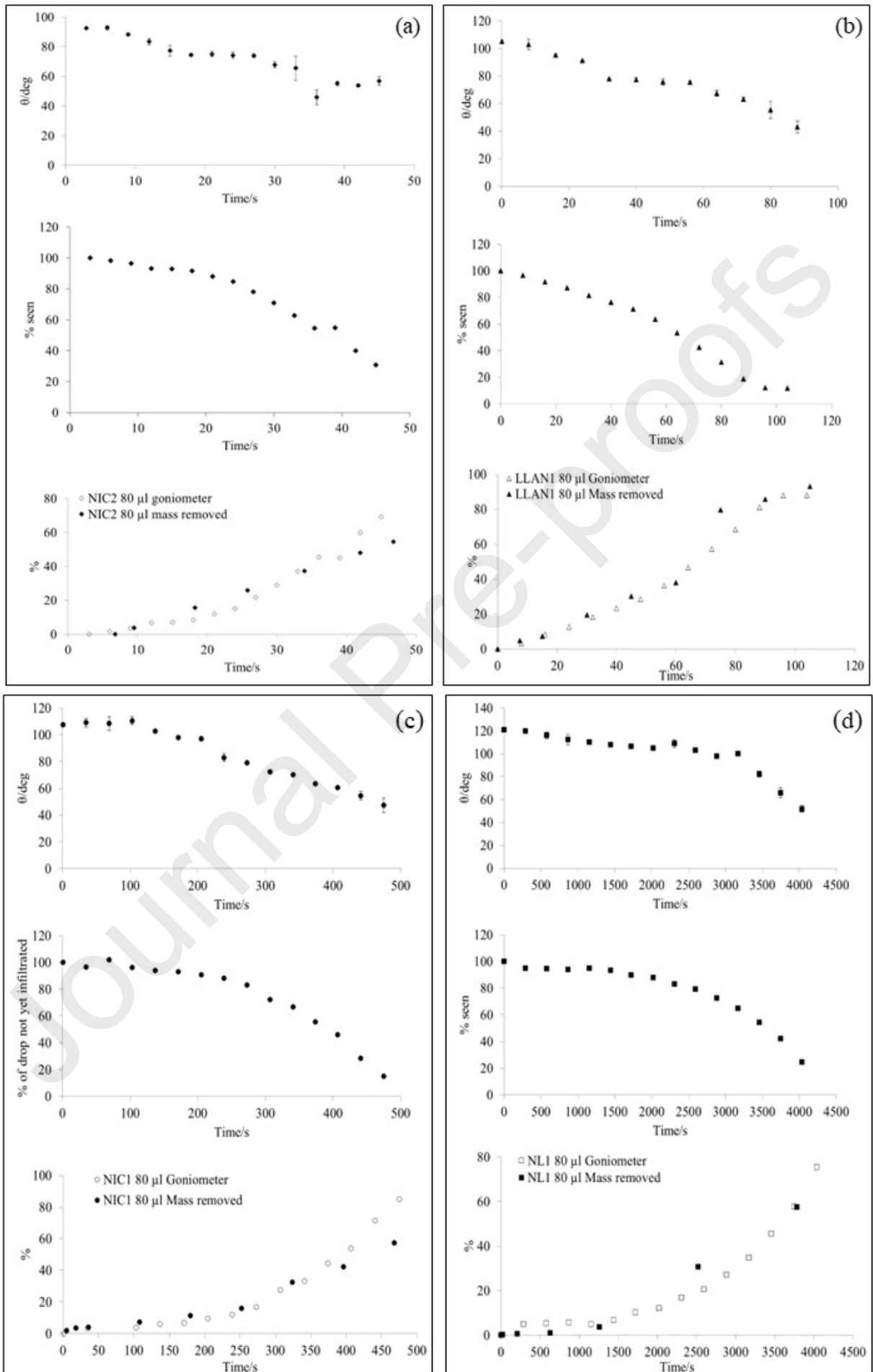
571 Figure 11 shows contact angle, fraction of water drop penetrated, and mass of soil wetted as a
 572 function of time for all soils studied. (Note the data set for mass removal is not directly
 573 comparable to that from the goniometer because the tests were carried out under different
 574 conditions; the mass removal experiments were conducted in a constant temperature/relative
 575 humidity room whereas the goniometer was restricted to the laboratory conditions where it was
 576 set up. Therefore, to make a meaningful comparison between data, the data has been adjusted
 577 by normalising the time axis for mass removal to give the same WDPT values as the goniometer
 578 experiments.)

579 In previous work we have shown that the measured contact angle for soils using a goniometer
 580 designed for flat surfaces is not the true contact angle for the soil–liquid interface but rather a
 581 composite made up of the true contact angle plus an additional term arising from how the water

582 drop sits on the soil surface (Balshaw et al., 2021). Even so, the variation in contact angle over
583 time gives some measure of the progress of the wetting process. Time-lapse images taken using
584 a goniometer, can also be used to provide a measurement of the volume of the water drop which
585 has not yet penetrated the soil over time.

586 The data is consistent with the model proposed in that all measurements show a process that
587 begins slowly but accelerates with time. For the water repellent soils NIC1 (severely) and NL1
588 (severely-extremely) in particular, there is a significant initial period of time during which there
589 is little change in any of the measured properties, a period of time we interpret as corresponding
590 to the transition from adhesional wetting to interstitial wetting as the most significant kinetic
591 barrier to the overall process, i.e. the transition from θ to θ_{critical} , is overcome.

592

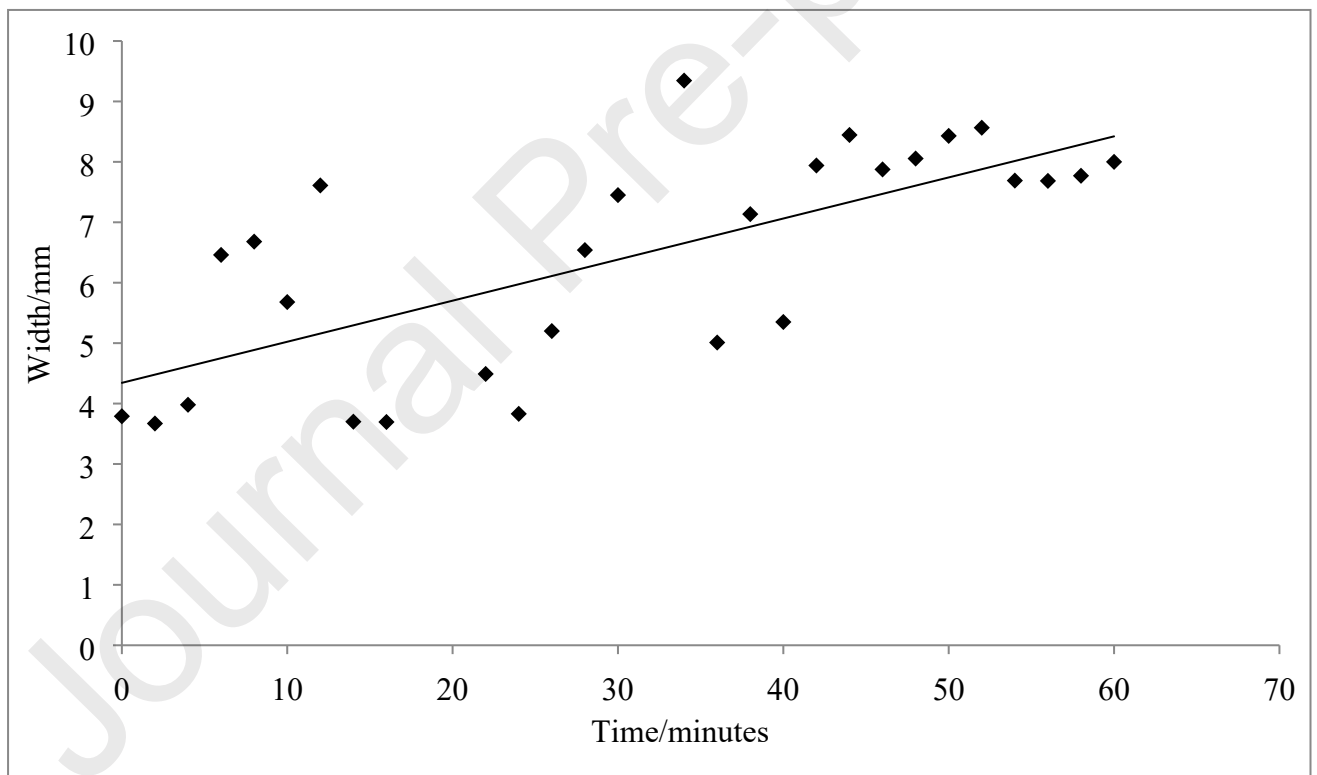


594 **Figure 11.** Contact angle, fraction of water drop penetrated, and mass of soil wetted as a
 595 function of time for (a) NIC2, (b) LLAN1, (c) NIC1, (d) NL1. 80 μl drops. In each instance:
 596 (Top) contact angle (θ) from time-lapse goniometer images against time. (Middle) Fraction of
 597 drop not yet infiltrated over time. (Bottom) Fraction of total mass removed against time, along
 598 with fraction of drop infiltrated against time, i.e. inverse of Middle plot, for comparison (data
 599 for mass removed adjusted to allow for same WDPT timescales, see text).

600

601 The rate of penetration is further increased by lateral spread of water in the soil, as shown in
 602 Figure 12. A comparison of the bulk water soil contact area before and after penetration for a
 603 100 μl drop on AUC (wetable) soil used to obtain the data in Figure 12, gives an initial contact
 604 circle area of $\pi(2.2)^2 = 15 \text{ mm}^2$, and a final contact area, assuming a spherical cap of 4 mm
 605 radius and height of 7 mm (after full penetration the depth of the pellet was 7 mm), of $\pi(4^2 +$
 606 $7^2) = 204 \text{ mm}^2$; i.e. a fourteen fold increase in bulk contact area, contact line, and hence rate of
 607 water penetration, at the end of the process compared to that at the start. This is consistent with
 608 the observation of an accelerating rate of penetration once the drop has broken through from
 609 the first contact layer into bulk soil.

610



611

612 **Figure 12.** Width of wetted soil pellet against penetration time, obtained using AUC (wetable)
 613 soil by measurement of frozen pellet obtained at specified time by immersion in liquid nitrogen.
 614 After full penetration the depth of the pellet was ca. 7 mm.

615

616 5. Conclusions and implications

617 From theoretical considerations of the energetics and kinetics of the processes by which a water
618 drop makes contact and then penetrates into soil, a three-stage model has been proposed,
619 advancing the understanding of how water eventually infiltrates water repellent soils. It
620 involves the following: 1) Adhesion wetting as soil and water first make contact, which is
621 essentially instantaneous on the time scale of our experiments. 2) A kinetic barrier transitional
622 stage in which molecular reorganisation of organics on soil reduces the contact angle from θ to
623 θ_{critical} which allows water to contact soil particles in layers below those initially in contact. The
624 time for this to occur depends on: θ and the rate of any molecular reorganisation required to
625 reduce θ to θ_{critical} , with the latter dependent upon particle size distribution and packing. 3)
626 Branching interstitial wetting as water infiltrates into the bulk soil. The time for this to occur
627 depends on θ , and the rate of any molecular reorganisation required to reduce θ to 90° .

628 Studies of optical microscopy, mass of soil initially wetted, penetration time through layers of
629 soil of different thicknesses, time-dependent measurements of contact angle, volume of water
630 penetrated, and mass of soil wetted, all give results consistent with this model. However, only
631 for highly water repellent soils can distinct stages in wetting be clearly resolved experimentally,
632 presumably because only these soils have a high enough kinetic barrier in the transitional stage
633 for good separation between stages. For less water repellent soils, while the general time
634 dependent behaviour remains consistent with the model, the distinction between the three
635 stages is not so easy to resolve.

636 The findings presented here have relevance to the amelioration of soil water repellency. Any
637 additive which increases packing density by increasing particle size heterogeneity would be
638 expected to lead to a reduction in θ_{critical} and it is suggested to contribute to the mechanism by
639 which the addition of clay or other fine particulates lowers soil water repellency (e.g. Cann et
640 al., 2000) is via a reduction in θ_{critical} , as fine particulates sit in between soil grains and reduce
641 the depth to which a water drop must sit on the soil before contacting underlying layers of soil
642 particles.

643

644 **Acknowledgements** Helen M. Balshaw thanks the Engineering and Physical Sciences
645 Research Council (EPSRC) Doctoral Training Academy (DTA) grant for funding
646 (EP/L504865/1).

647

648 References

649 Balshaw, H.M. 2019. New approaches to the study of hydrophobicity and wetting of soils:
650 methods and theories. PhD Thesis. Swansea University, Swansea.

651

652 Balshaw, H.M., Douglas, P. and Doerr S.H. 2021. On the cause and correction of the
653 anomalously high contact angles measured on soils and granular materials. *Geoderma*, 391,
654 114973.

655

- 656 Bisdom, E.B.A., Dekker, L.W. and Schoute, J.F.T. 1993. Water repellency of sieve fractions
657 from sandy soils and relationships with organic material and soil structure. *Geoderma*. 56, 105-
658 118.
- 659
- 660 Bond, R.D. 1972. Germination and yield of barley when grown in a water-repellent
661 sand. *Agronomy Journal*, 64, 402–403
- 662
- 663 Cann, M.A. 2000. Clay spreading on water repellent sands in the south east of South Australia
664 – promoting sustainable agriculture. *Journal of Hydrology*. 231-232, 333-341.
- 665
- 666 Chang, H. and Wang, L. 2010. A Simple Proof of Thue's Theorem on Circle Packing.
667 <https://arxiv.org/abs/1009.4322v1> - accessed February 2019.
- 668
- 669 Dekker, L.W. and Ritsema, C.J., 1994. How water moves in a water repellent sandy soil. 1.
670 Potential and actual water repellency. *Water Resources Research*. 30, 2507- 2517.
- 671
- 672 Dekker, L.W. and Ritsema, C.J. 1996. Variation in water content and wetting patterns in Dutch
673 water repellent peaty clay and clayey peat soils. *Catena*. 28, 89- 105.
- 674
- 675 Dekker, L.W., Ritsema, C.J. and Oostindie, K. 2000. Extent and significance of water
676 repellency in dunes along the Dutch coast. *Journal of Hydrology*. 231-232, 112-125.
- 677
- 678 Diehl, D. and Schaumann, G.E. 2007. The nature of wetting on urban soil samples: wetting
679 kinetics and evaporation assessed from sessile drop shape. *Hydrological Processes*. 21, 2255–
680 2265.
- 681
- 682 Doerr, S.H. 1998. On Standardizing the 'water drop penetration time' and the 'molarity of an
683 ethanol droplet' techniques to classify soil hydrophobicity: a case study using medium textured
684 soil. *Earth Surface Processes and Landforms* 23, 663- 668.
- 685
- 686 Doerr, S.H., Shakesby, R.A. and Walsh, R.P.D. 1998. Spatial variability of soil hydrophobicity
687 in fire-prone eucalyptus and pine forests, Portugal. *Soil Science*. 163, 313-324.
- 688

- 689 Doerr, S.H., Shakesby, R.A. and Walsh, R.P.D. 2000. Soil water repellency: its causes,
690 characteristics and hydro-geomorphological significance. *Earth Science Reviews*. 51, 33-65.
- 691
- 692 Doerr, S.H., Dekker, L.W., Ritsema, C.J., Shakesby, R.A. and Bryant, R. 2002. Water
693 repellency of soils: the influence of ambient relative humidity. *Soil Science Society of America*
694 *Journal*. 66, 401-405.
- 695
- 696 Doerr, S.H., Llewellyn, C.T., Douglas, P., Morley, C.P., Mainwaring, K.A., Haskins, C.,
697 Johnsey, L., Ritsema, C.J., Stagnitti, F. and Allinson, G. 2005. Extraction of compounds
698 associated with water repellency in sandy soils of different origin. *Australian Journal of Soil*
699 *Research*. 43 (3), 225-237.
- 700
- 701 Douglas, P., Mainwaring, K.A., Morley, C.P., Doerr, S.H. 2007. The kinetics and energetics
702 of transitions between water repellent and wettable soil conditions: a linear free energy analysis
703 of the relationship between WDPT and MED/CST. *Hydrological Processes*. 21, 2248-2254.
- 704
- 705 Franco, C.M.M., Clarke, P.J., Tate, M.E. and Oades, J.M. 2000. Hydrophobic properties and
706 chemical characterisation of natural water repellent materials in Australian sands. *Journal of*
707 *Hydrology*. 231-232, 47-58.
- 708
- 709 Hallett, P.D., Douglas, J.T., Ritz, K., Wheatley, R.E. and Young, I.M. 2001. Plant root and
710 microbial derived soil water repellency. In: *Scottish Crop Research Institute Annual Report*
711 *2000/2001* (Macfarlane-Smith, W.H. and Heilbronn, T., editors), 148- 151.
- 712
- 713 Jaycock, J. and Parfitt, G. 1981. *Chemistry of interfaces*. Ellis Horwood series in
714 *chemical science*. Chichester, England.
- 715
- 716 Jex, G.W., Bleakley, B.H., Hubbell, D.H. and Munro, L.L. 1985. High humidity induced
717 increase in water repellency in some sandy soils. *Soil Science Society of America Journal*. 49,
718 1177-1182
- 719
- 720 Letey, J. 1969. Measurement of contact angle, water drop penetration time, and critical surface
721 tension. In: DeBano, L.F., Letey, J. (Eds.), *Proceedings of a Symposium on Water Repellent*
722 *Soils*, May 6-10. 1968, Riverside, CA, pp. 43-47, 354p.
- 723

724 Letey, J., Carrillo, M.L.K. and Pang, X.P. 2000. Approaches to characterize the degree of water
725 repellency. *Journal of Hydrology*, 231-232, 61-65.

726

727 McGhie, D.A. and Posner, A.M. 1981. The effect of plant top material on the water
728 repellence of fired sands and water-repellent soils. *Australian Journal of Agricultural*
729 *Research*. 32, 609-620.

730

731 McIntosh, J.C. and Horne, D.J. 1994. Causes of repellency: I. The nature of the hydrophobic
732 compounds found in a New Zealand development sequence of yellow brown sands. In:
733 *Proceedings of the 2nd National Water Repellency Workshop, August 1994, Perth, Western*
734 *Australia*, pp. 8-12.

735

736 Rigby, M., Smith, E.B., Wakeham, W.A., and Maitland, G.C. 1986. *The Forces Between*
737 *Molecules*. Clarendon Press, Oxford.

738

739 Ritsema, C.J. and Dekker, L.W. 1996. Water repellency and its role in forming preferred flow
740 paths in soils. *Australian Journal of Soil Research*. 34, 475-487.

741

742 Roberts, F.J. and Carbon, B.A. 1972. Water repellence in sandy soils of southwestern
743 Australia. 2. Some chemical characteristics of the hydrophobic skins. *Australian Journal of*
744 *Soil Research*. 10, 35-42.

745

746 Shirtcliffe, N.J., McHale, G., Newton, M.I., Pyatt, F.B. and Doerr, S.H. 2006. Critical
747 conditions for the wetting of soils, *Applied Physical Letters*. 89 art. 09410.

748

749 Wolfram Mathworld, 2019. <http://mathworld.wolfram.com/SphericalCap.html> - accessed
750 February 2019.

751

752 **Abstract**

753 Water repellent behaviour of soils is a widely studied phenomenon given its implications for
754 infiltration, runoff, erosion and preferential flow. However, the principles underlying the
755 eventual penetration of water into affected soils remain poorly understood. Theoretical
756 considerations of the energetics and kinetics involved as a water drop makes contact with a
757 water repellent soil surface and eventually penetrates into the soil suggest three distinct stages
758 in the overall process. These stages are 1) adhesional wetting as soil and water first make

759 contact, followed by 2) a kinetic barrier transitional stage in which molecular reorganisation
760 of organics on soil reduces the water-soil contact angle to allow the water drop to sit deeper
761 over soil particles of initial contact such that there is contact with particles in directly
762 underlying soil layers, and finally 3) branching interstitial wetting as water penetrates into the
763 bulk soil. Studies presented here of optical microscopy, mass of soil initially wetted,
764 penetration time through layers of soil of different thicknesses, and time-dependent
765 measurements of contact angle, volume of water penetrated, and mass of soil wetted, all give
766 results consistent with this model. However, only for highly water repellent soils can distinct
767 stages in wetting be clearly resolved experimentally, presumably because only these soils
768 have a high enough kinetic barrier in the transitional stage for good separation between
769 stages. For less water repellent soils, while the general time dependent behaviour remains
770 consistent with the model, the distinction between the three stages is not so easy to resolve
771 experimentally. The roles of contact angle, particle size distribution and drop size in
772 determining the rates of these stages is considered, and the implications of the model for
773 understanding soil water repellency are discussed.

774

775 **Declaration of interests**

776

777 The authors declare that they have no known competing financial interests or personal
778 relationships that could have appeared to influence the work reported in this paper.

779

780 The authors declare the following financial interests/personal relationships which may be
781 considered as potential competing interests:

782

783

784

785

786

787

788

789 **Helen Balshaw:** Conceptualization Methodology, Formal Analysis, Investigation
790 Writing - Original Draft, Writing - Review & Editing

791 **Peter Douglas:** Conceptualization, Writing - Original Draft, Writing - Review &
792 Editing

793 **Stefan Doerr:** Writing - Original Draft, Writing - Review & Editing

794

795

796

797 **Figure 1** Experimental set-up for (a) mass removal and (b) sinter based water drop penetration
798 time studies. (a) Schematic of cotton bud being brought into contact with a water drop (top)

799 and example of mass removed sample using the cotton bud method (bottom). (b) Image
 800 showing soils of varying thickness on top of a glass sinter disc.
 801

802 **Figure 2** Gibbs energy change for the loss of liquid-vapour interface and increase of solid-
 803 liquid interface as a soil grain penetrates into the surface of a water drop for a single spherical
 804 particle. **a)** Wetting of a spherical particle as it is taken into a water drop to depth d . **b)** Gibbs
 805 energy change (J) for a single soil particle of 0.15 mm radius penetrating into a 100 μl drop
 806 (mm) during the wetting process, all with particle radius of 0.15mm and (i) where $\theta = 45^\circ$, (ii)
 807 where $\theta = 90^\circ$ and (iii) where $\theta = 135^\circ$. Where: the Gibbs energy change from the loss of
 808 liquid-vapour interface is given as a dotted line; the Gibbs energy change for the increase of
 809 solid-liquid interface is given as a solid line; and the overall Gibbs energy change
 810 (summation of previous two terms) is given as a dashed line. The particle will penetrate the
 811 water drop to the point where $(\partial G/\partial(\text{depth})) = 0$, i.e. the slope of the dashed line in the
 812 diagram is zero.

813

814 **Figure 3** Gibbs energy change (J) for a single sheet of close-packed particles, with depth of
 815 particle penetration into the drop (mm) during the wetting process, where $\theta = 111^\circ$, drop
 816 volume and particle radius of 0.15 mm for drop size 100 μl showing the gravity term as a long
 817 dash. Where: the Gibbs energy gained from the loss of liquid-vapour interface is given as a
 818 dotted line; the Gibbs energy gained by the increase of solid-liquid interface is given as a solid
 819 line and the overall Gibbs energy (summation of terms) is given as a dashed line.

820 **Figure 4** Dependence of the depth of water drop penetration upon (a) drop volume and (b)
 821 contact angle for a water drop on close-packed spheres. **a)** Depth of the water drop on close-
 822 packed spheric particles of 0.15 mm radius against drop volume for $\theta = 111^\circ$ (the contact angle
 823 for paraffin wax on a flat surface). **b)** Depth of water penetration against soil contact angle (θ)
 824 for 100 μl drop on 0.3 mm diameter particles (The dashed lined shows the $0.15 \times 1.63r$ (0.245
 825 mm) penetration depth, and corresponding theta of 50 degrees).

826

827 **Figure 5.** Cross-sectional profiles from profilometer measurements on UKC soil showing
 828 surface roughness; 10 mm long scans at 25 μm spaced intervals, with 400 μm vertical scale
 829 marker shown. Approximate diameters of the contact circles for 20 and 50 μl drop on NIC2
 830 (orange) which is a strongly repellent soil, and NL1 (red) which is a severely-extremely
 831 repellent soils, obtained from goniometer images, are also shown.

832

833 **Figure 6.** Schematic of water drop sitting on soil grains. Branching interstitial wetting and
 834 penetration into bulk soil cannot occur until hatched area undergoes a change in hydrophobicity
 835 to permit water flow. The movement of water from the depth from where the water drop is
 836 initially sitting on the grains to the critical depth where it reaches the second layer of grains is
 837 controlled by this change in θ to θ_{critical} .

838

839 **Figure 7.** Schematic showing the proposed wetting processes in a water repellent soil.

840

841 **Figure 8.** Optical microscopy image of water drop (20 μl) on NIC1 soil showing the adhesional
842 stage of wetting process with grains adhered to the drop surface.

843 **Figure 9.** Initial volume of soil (mm^3) per mm^2 of water drop against log water drop penetration
844 time for NIC2 (strongly) (orange) and LLAN1 (strongly) (green) NIC1 (severely) (blue), and
845 NL1 (severely–extremely) (red). Triangle (20 μl), diamond (50 μl), circle (80 μl) square (100
846 μl) soils at different drop volumes. The curve has been included just as a guide for the eye.

847

848 **Figure 10.** Global plot of sinter water drop penetration time data, based on an average
849 measurement from three drops per data point. (a) NIC2 (b) LLAN1 (c) NIC2 (d) NL1. Where,
850 20 μl is a triangle and corresponding linear line is dotted, 30 μl is a dash and corresponding
851 linear line is dash dot dot, 50 μl is a diamond and corresponding linear line is dash and 80 μl
852 is a circle and corresponding linear line is solid.

853

854 **Figure 11.** Contact angle, fraction of water drop penetrated, and mass of soil wetted as a
855 function of time for (a) NIC2, (b) LLAN1, (c) NIC1, (d) NL1. 80 μl drops. In each instance:
856 (Top) contact angle (θ) from time-lapse goniometer images against time. (Middle) Fraction of
857 drop not yet infiltrated over time. (Bottom) Fraction of total mass removed against time, along
858 with fraction of drop infiltrated against time, i.e. inverse of Middle plot, for comparison (data
859 for mass removed adjusted to allow for same WDPT timescales, see text).

860

861 **Figure 12.** Width of wetted soil pellet against penetration time, obtained using AUC (wetable)
862 soil by measurement of frozen pellet obtained at specified time by immersion in liquid nitrogen.
863 After full penetration the depth of the pellet was ca. 7 mm.

864

865

866 Highlights

- 867 1) Three-step model: adhesion wetting; molecular reorganisation; interstitial wetting
- 868 2) Experimental studies give results consistent with this model
- 869 3) Has implications for water repellency amelioration using particulate additives

870

871